Electronic Supplementary Material (ESI) for Metallomics.


## Supporting Information

# Coordinative unsaturated $Cu^{I}$ entities are crucial intermediates governing cell internalization of copper. A combined experimental and DFT study.

Silvia Carlotto,*[a] Arkadiusz Bonna,[b] Karolina Bossak-Ahmad,[c] Wojciech Bal,[c] Marina Porchia,[d] Maurizio Casarin,[a] and Francesco Tisato,*[d]

**Experimental Section**

**General.**

*N,N,N',N'*-Tetramethyl-*O*-(1*H*-benzotriazol-1-yl)uronium hexafluorophosphate (HBTU), diisopropylethylamine (DIPEA), piperidine, triisopropylsilane (TIS) and dithiotreitol (DTT)and trifluoroacetic acid (TFA) were purchased from Merck. Dimethylformamide was purchased from Roth. Fmoc amino acids derivatives were purchased from Novabiochem. Tenta Gel S RAM was purchased from RAPP Polymere. Automated Peptide Synthesizer Prelude™ was purchased from Protein Technologies, Inc.

**Synthesis of model peptides.**

The peptides **mimicking portions of hCtr1** contain a terminal free amine function at M (G for GGH), and an amidated C-terminus at H (S for hCtr1_10) that is: MDH-am (hCTR1_3), MDHSHH-am (hCTR1_6), and MDHSHHMGMS-am (hCTR1_-10). They were synthesized on a Prelude™ peptide synthesizer according to the Fmoc strategy on the solid phase using Tenta Gel S RAM resin as a solid phase, HBTU and DIPEA for coupling of Fmoc amino acid derivatives, and 20% Piperidine in DMF as a Fmoc-deprotection agent. Release of fully deprotected peptides was achieved by using of cocktail of 94% TFA with TIS, DTT and water (95:1:2.5:2.5). Released peptides were precipitated directly from the TFA solutions by the addition of cold diethyl ether. Next, ether was decanted and peptides were dried, dissolved in water and lyophilized. Crude peptides were analyzed by HPLC on a Breeze system (Waters) equipped with an ACE5 C18-300 analytical column (5 μm particle size, 4.6 × 250 mm) followed by analysis on ESI-MS (Q-Tof Premier mass spectrometer, Waters.

**Purification of peptides.**

Synthesized peptides were purified by means of a reverse-phase HPLC (Breeze, Waters) equipped in dual-length UV-vis detector (settings of 220 nm and 280 nm) with the use of Vydac semi-preparative column (5 mm particle size, 10 × 250 mm). Eluting solvent A was 0.1 % (v/v) trifluoroacetic (TFA) in water, and B 0.1% TFA in 90% acetonitrile (v/v). The purity of the collected peptides was checked via Q-Tof Premier mass spectrometer (Waters).

**MS measurements.**

Mass spectra were collected using a LCQ Fleet ion trap mass spectrometer (Thermo-Scientific) equipped with an ESI source operating in positive ion mode.

Each model peptide, $[Cu^{I}(PTA)_4][BF_4]$ or $CuCl_2$ were separately dissolved in 1 mL of milliQ water at autogenous pH (*ca*. 5.5) giving *ca.* $10^{-2}$ M stock solutions. 1 μL of each model peptide solution was subsequently diluted 1:1000 v:v with MeOH to obtain *ca.* $10^{-5}$ M water/methanol solutions. Each diluted model peptide solution was then treated with four-fold molar excess of $[Cu^{I}(PTA)_4][BF_4]$ or $Cu^{II}Cl_2$ (few μLs). Selected experiments were performed replacing $[Cu^{I}(PTA)_4][BF_4]$ for $[Ag^{I}(PTA)_4][BF_4]$ and using the identical procedure adopted for the isostructural copper(I) compound, *i.e.* model peptides and $[Ag^{I}(PTA)_4][BF_4]$ were dissolved in 1mL of milliQ water and diluted 1:1000 v:v with MeOH to give *ca.* $10^{-5}$ M water/methanol

solutions. Each diluted model peptide solution was then treated with four-fold molar excess of $[Ag^{I}(PTA)_4][BF_4]$. The mixed solutions were left to stand 2 min at room temperature, and then directly infused into the ESI source via a syringe pump at a flow rate of 10 μL/min. The ions were produced using a spray voltage of 3.5 kV and entrance capillary temperature of 280°C. Other instrumental parameters were automatically adjusted to optimize the signal-to-noise ratio. Tandem mass spectrometric ($MS^n$) experiments were performed by resonant excitation of the ion of interest through a supplementary radiofrequency (rf) voltage in the range 10–35% of its maximum value (5 V peak-to-peak). The isolation width was set at 4 mass units for apopeptides, at 6 mass units for copper compounds and at 8 mass units for silver compounds.

Full ESI(+)MS spectra and $MS^n$ experiments on $[Ag^{I}(peptide)]^+$ adducts gave results qualitatively superimposable with those detected on $[Cu^{I}(peptide)]^+$ ions.

Some experiments have been performed with monoisotopic $^{63}CuCl_2$ or monoisotopic $^{65}CuCl_2$ obtained from Trace Sciences International as dihydrate salts, using the procedure adopted for naturally occurring mixture of $^{63/65}Cu$ isotopes.

**DFT calculations Details.**

DFT spin-unrestricted calculations have been carried out by using the 2014 release of the ADF package [1]. The adopted exchange-correlation (XC) functional is based on the parameterization of the electron gas data provided by Vosko, Wilk and Nusair [2], as far as the LDA component is concerned, while the Becke, Perdew and Wang gradient corrections have been used for the exchange part (BP86) [3],[4]. All electrons triple-ζ with a single polarization function (TZP) Slater-type orbitals have been employed for all elements.


[1] Amsterdam Density Functional (ADF) version 2014.01. http://www.scm.com.
[2] S. H. Vosko, L. Wilk, M. Nusair, Can. J. Phys. 58 (1980) 1200.
[3] A. D. Becke, Physical Review A 38 (1988) 3098.
[4] J. P. Perdew, Y. Wang, Physical Review B 33 (1986) 8822.


*$[Cu^{I}(h\text{-}Ctr1\text{-}3)]^+$ local minima*. The AM is associated to a quasi-linear $Cu^{I}$ coordination, involving the terminal amino function of Met and the imidazole N of His (see Figure ESI3A). As far as the three local minima are concerned, one is associated to a further $Cu^{I}$ quasi-linear coordination ($NH_2$-$Cu^{I}$-O, +11 Kcal/mol) (see Figure ESI3C), while the remaining two imply $Cu^{I}$ trigonal arrangements with the metal ion coordinated either to two nitrogen and one oxygen atoms (+3 kcal/mol, see Figure ESI3B) or to nitrogen, oxygen and sulfur atoms (+11 kcal/mol, see Figure ESI3D).

*$[Cu^{I}(h\text{-}Ctr1\text{-}6)]^+$ local minima*. Similarly to $[Cu^{I}(h\text{-}Ctr1\text{-}3)]^+$, the $Cu^{I}$ environment corresponding to the AM perfectly matches the one ($(Met)H_2N$-$Cu^{I}$-N(His)) obtained for the simpler tripeptide (see Figure ESI4A). As far as the remaining two sites are concerned, they lay at +20 and +57 kcal/mol from the AM, with the former associated to a coordination of two central His residues to $Cu^{I}$ and the latter with $Cu^{I}$ in between SHH (see Figure ESI4C and ESI4B, respectively).

*$[Cu^{I}(h\text{-}Ctr1\text{-}10)]^+$ local minima*. Even though, the AM implies again a linearly coordinated $Cu^{I}$ ion, its environment does not correspond to the one obtained both for the $[Cu^{I}(h\text{-}Ctr1\text{-}3)]^+$ and $[Cu^{I}(h\text{-}Ctr1\text{-}6)]^+$. The $[Cu^{I}(h\text{-}Ctr1\text{-}10)]^+$ AM is associated to a (His)N-$Cu^{I}$-N(His) fragment and it involves the HSH residues (see Figure ESI6B). Incidentally, the other local minima (four) are associated to an almost linear MDH N-$Cu^{I}$-N

(+18 kcal/mol, see Figure ESI6A), HH N-$Cu^{I}$-N (+18 kcal/mol, see Figure ESI6C) and HM N-$Cu^{I}$-S (+21 kcal/mol, see Figure ESI6D) coordination. As far as the fourth minimum is concerned, it is characterized by a MGM trigonal coordination (+32 kcal/mol) (see Figure ESI6E).

Figure captions:

Figure S1. Full ESI(+)MS spectrum of $[Cu(PTA)_4]^+$ in water/methanol solution.

Figure S2. Full ESI(+)MS spectrum of $[Cu^{I}(hCtr1\_3)]^+$ (A), $[Cu^{I}(hCtr1\_6)]^+$ (B) and $[Cu^{I}(hCtr1\_10)]^+$ (C).

Figure S3. Optimized structures computed for $[Cu^{I}(hCtr1\_3)]+$. The energy differences (ΔE) are reported in kcal/mol and the bond lengths are in Å. The colour code for atoms is: Cu/green, O/red, S/yellow, C/blue, N/violet and H/white.

Figure S4. Optimized structures computed for $[Cu^{I}(hCtr1\_6)]^+$. The energy differences (ΔE) are reported in kcal/mol and the bond lengths are in Å. The colour code for atoms is: Cu/green, O/red, S/yellow, C/blue, N/violet and H/white.

Figure S5. Fragmentation scheme of $[Cu^{I}(hCtr1\_6)]^+$ at m/z 824.

Figure S6. Optimized structures computed for $[Cu^{I}(hCtr1\_10)]^+$. The energy differences (ΔE) are reported in kcal/mol and the bond lengths are in Å. The colour code for atoms is: Cu/green, O/red, S/yellow, C/blue, N/violet and H/white.

Figure S7a. $MS^n$ profile of $[Cu^{I}(hCtr1\_10)]^+$ at m/z 1230. Fragmentation via the product ion at m/z 984.

Figure S7b. $MS^n$ profile of $[Cu^{I}(hCtr1\_10)]^+$ at m/z 1230. Fragmentation via the product ion at m/z 807.

Figure S8. Full ESI(+)MS spectrum of $[Cu^{II}(hCtr1\_3) - H^+]^+$ (A), $[Cu^{II}(hCtr1\_6) - H^+]^+$ (B) and $[Cu^{II}(hCtr1\_10) - H^+]^+$ (C).

Figure S9. Optimized structure computed for $[Cu^{II}(GGH)]^+$. The bond lengths are in Å and the colour code for atoms is: Cu/green, O/red, C/blue, N/violet and H/white.

Figure S10. Clusters ions obtained after treatment of h-Ctr1_10 with: i) monoisotopic $^{63}Cu^{II}Cl_2$ (top trace, left) or ii) monoisotopic $^{65}Cu^{II}Cl_2$ (top trace, right). Bottom traces display the clusters after reduction of $Cu^{II}$ solutions with ascorbic acid.

Figure S11. Fragmentation scheme of $[Cu^{II}(hCtr1\_10) - H^+]^+$ at m/z 1229.

Figure S12. Fragmentation pathway of $[Cu^{II}(hCtr1\_3) - H^+]^+$ at m/z 462 under ESI(+)MS conditions (left); fragmentation pathway of $[Cu^{II}(hCtr1\_3) - 3H^+]^-$ at m/z 460 under ESI(-)MS conditions (right). Double arrows indicate fragmentation processes occurring with reduction of $Cu^{II}$ to $Cu^{I}$ and release of peptidic fragments as $(\text{radical cations})^{+\cdot}$.

Figure S1.

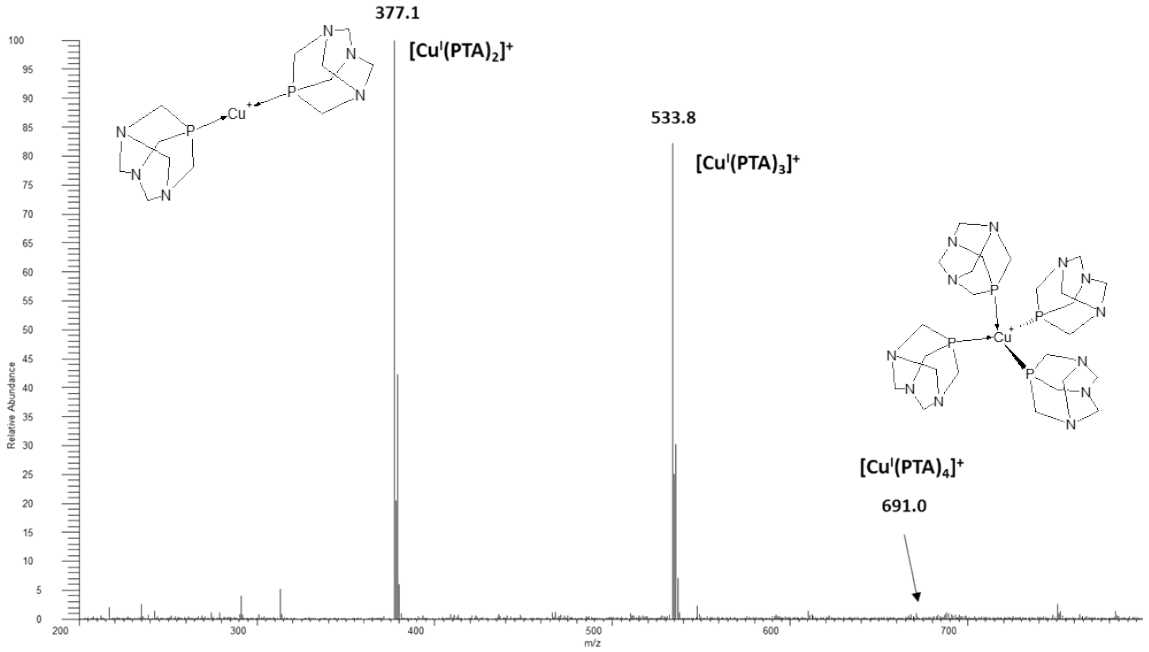
377.1
[Cu$^{I}$(PTA)$_2$]$^+$
533.8
[Cu$^{I}$(PTA)$_3$]$^+$
[Cu$^{I}$(PTA)$_4$]$^+$
691.0
Relative Abundance
m/z

Figure S2.

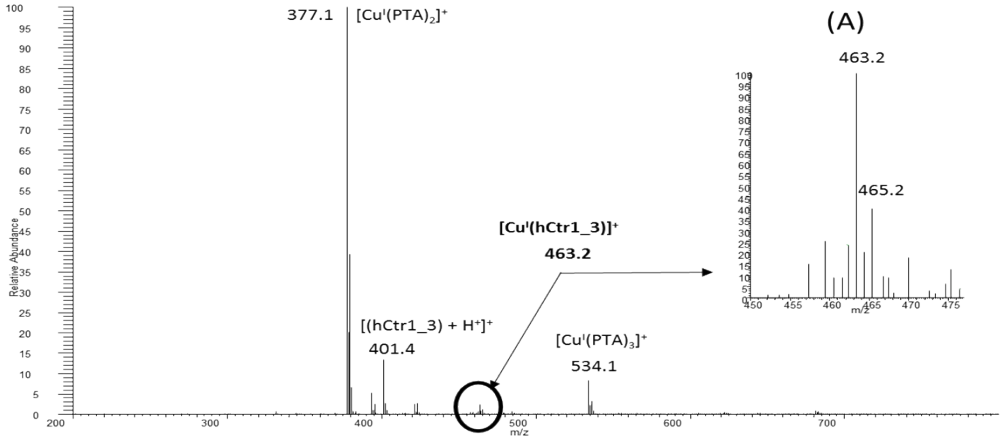
(A)
377.1 [Cu$^{I}$(PTA)$_2$]$^+$
463.2
465.2
[Cu$^{I}$(hCtr1_3)]$^+$
463.2
[(hCtr1_3) + H$^+$]$^+$
401.4
[Cu$^{I}$(PTA)$_3$]$^+$
534.1
Relative Abundance
m/z

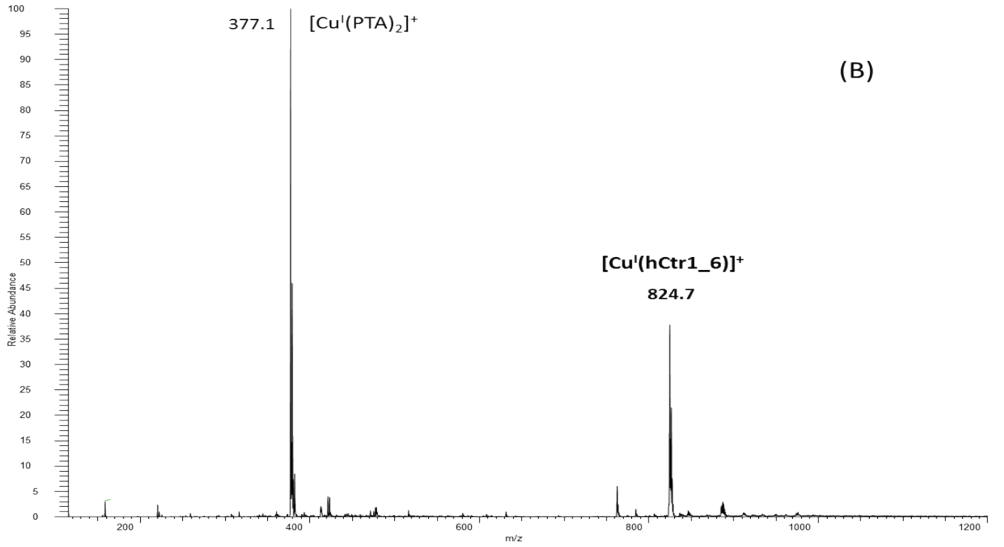
(B)
377.1 [Cu$^{I}$(PTA)$_2$]$^+$
[Cu$^{I}$(hCtr1_6)]$^+$
824.7
Relative Abundance
m/z

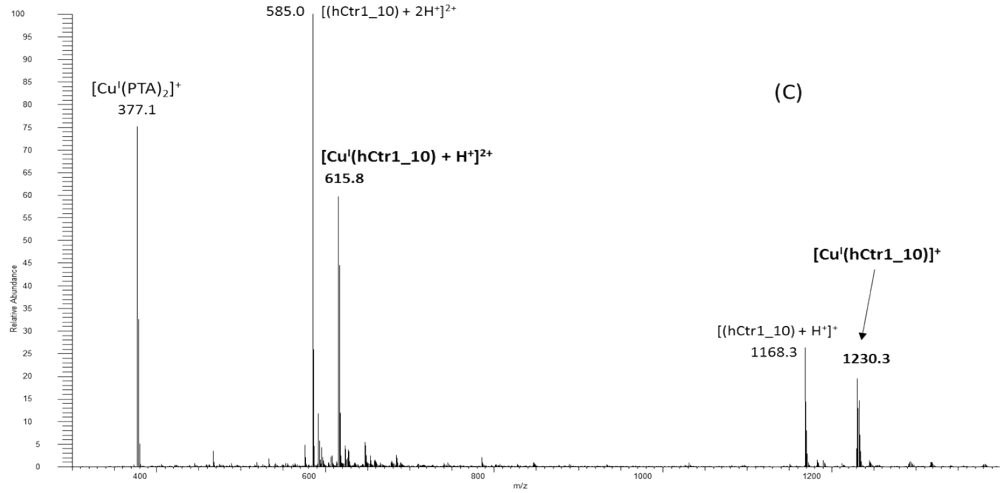
(C)
585.0 [(hCtr1_10) + 2H$^+$]$^{2+}$
[Cu$^{I}$(PTA)$_2$]$^+$
377.1
[Cu$^{I}$(hCtr1_10) + H$^+$]$^{2+}$
615.8
[Cu$^{I}$(hCtr1_10)]$^+$
[(hCtr1_10) + H$^+$]$^+$
1168.3
1230.3
Relative Abundance
m/z

Figure S3.

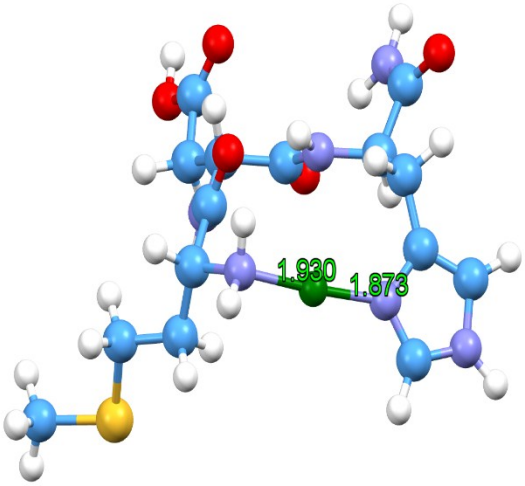


A. ΔE = 0 kcal/mol

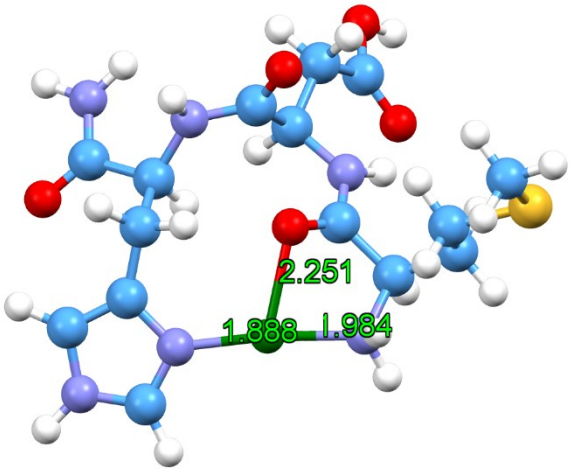


B. ΔE = 3.2 kcal/mol

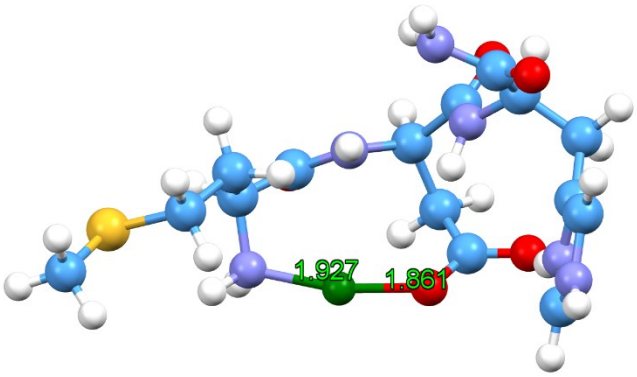


C. ΔE = 11.2 kcal/mol

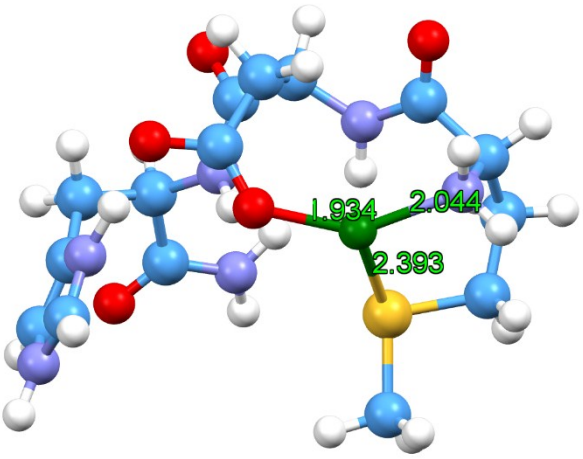


D. ΔE = 11.4 kcal/mol

Figure S4.

| | |
|---|---|
| 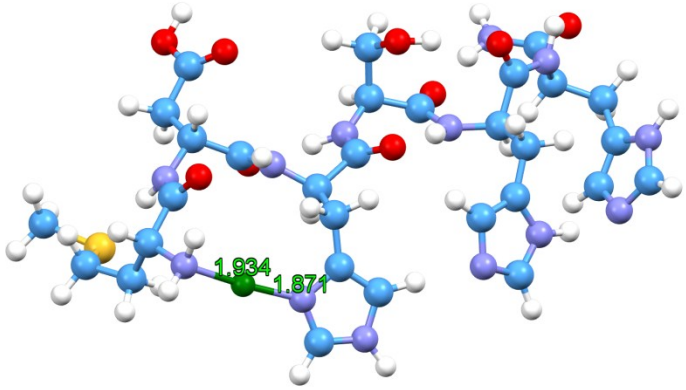 | A (site 1). ΔE = 0 kcal/mol |
| 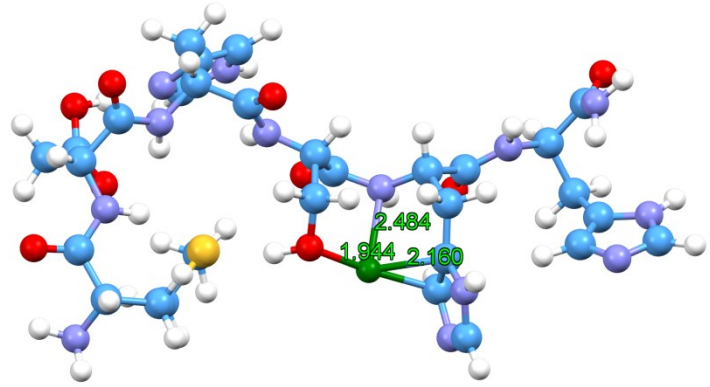 | B (site 2). ΔE = 57.6 kcal/mol |
| 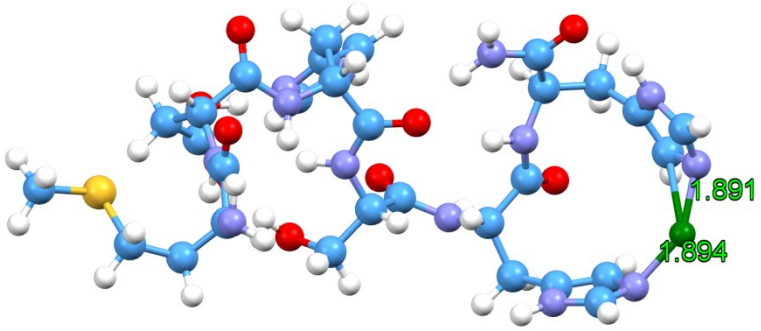 | C (site 3). ΔE = 20.0 kcal/mol |

Figure S5.

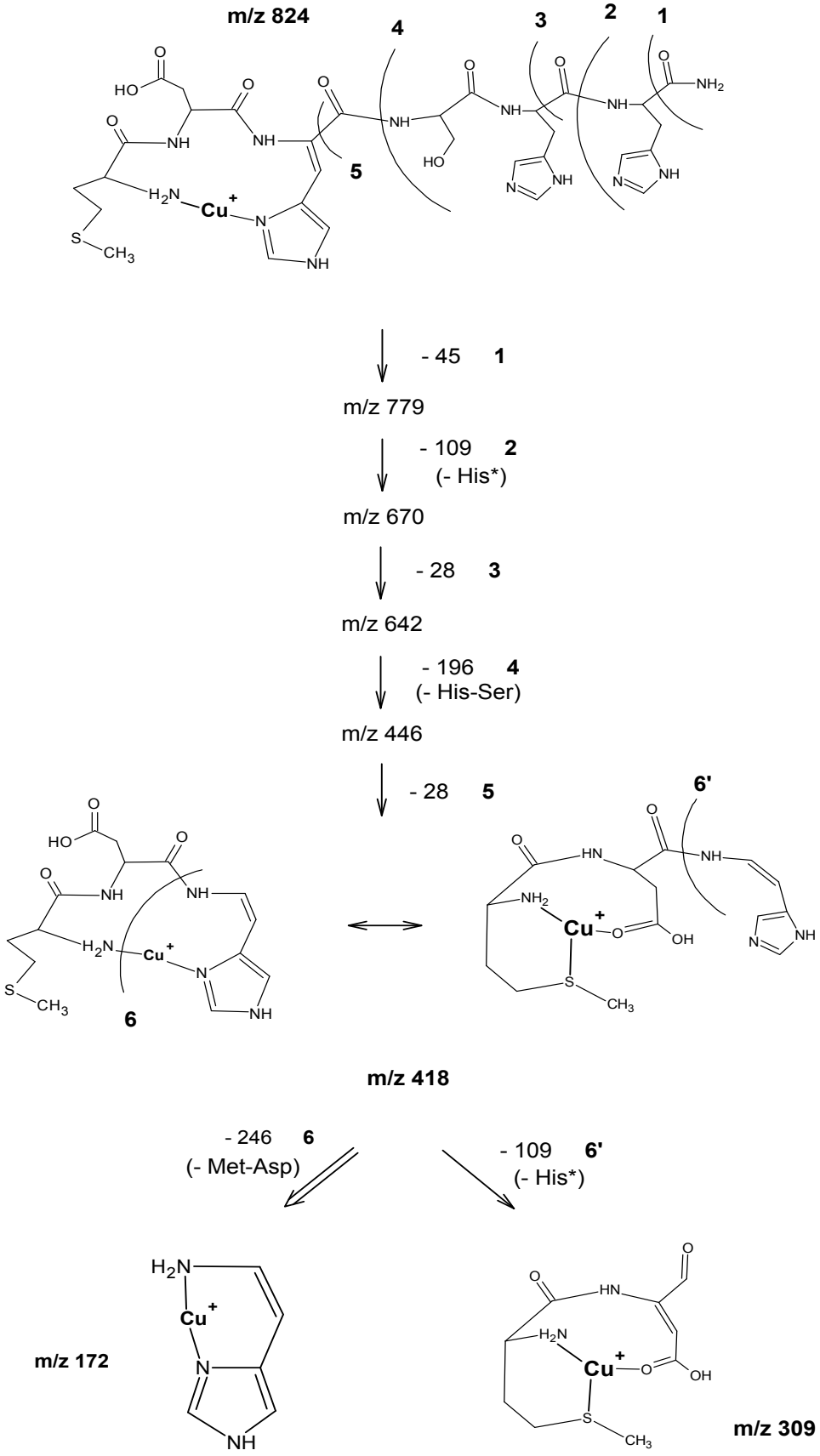
m/z 824
4
3
2
1
5
- 45 1
m/z 779
- 109 2
(- His*)
m/z 670
- 28 3
m/z 642
- 196 4
(- His-Ser)
m/z 446
- 28 5
6'
6
m/z 418
- 246 6
(- Met-Asp)
- 109 6'
(- His*)
m/z 172
m/z 309

Figure S6.

| | |
|---|---|
| 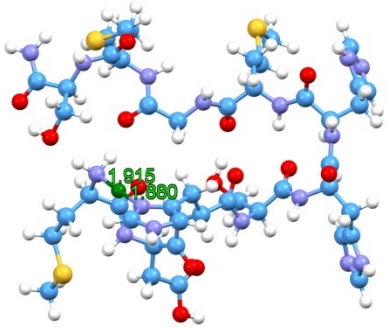 | A (site 1). ΔE = 18.0 kcal/mol |
| 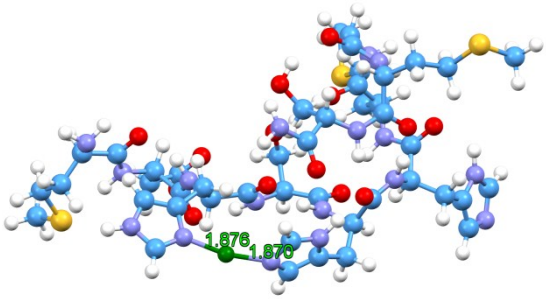 | B (site 2). ΔE = 0 kcal/mol |
| 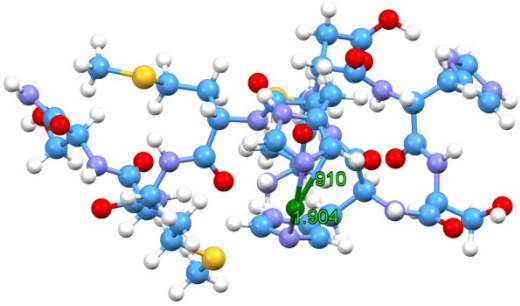 | C (site 3). ΔE = 18.5 kcal/mol |
| 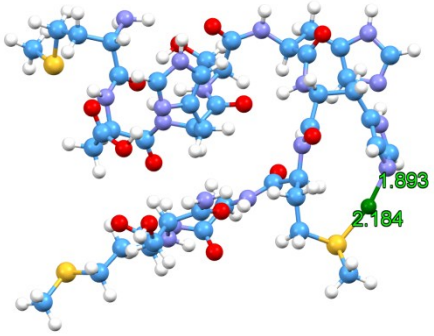 | D (site 4). ΔE = 20.5 kcal/mol |
| 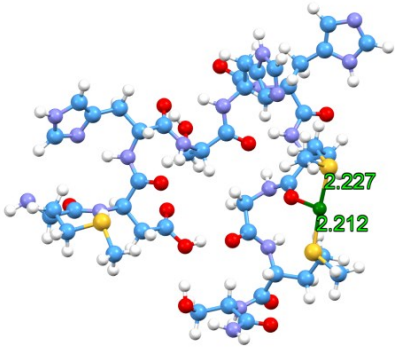 | E (site 5). ΔE = 31.8 kcal/mol |

Figure S7a.

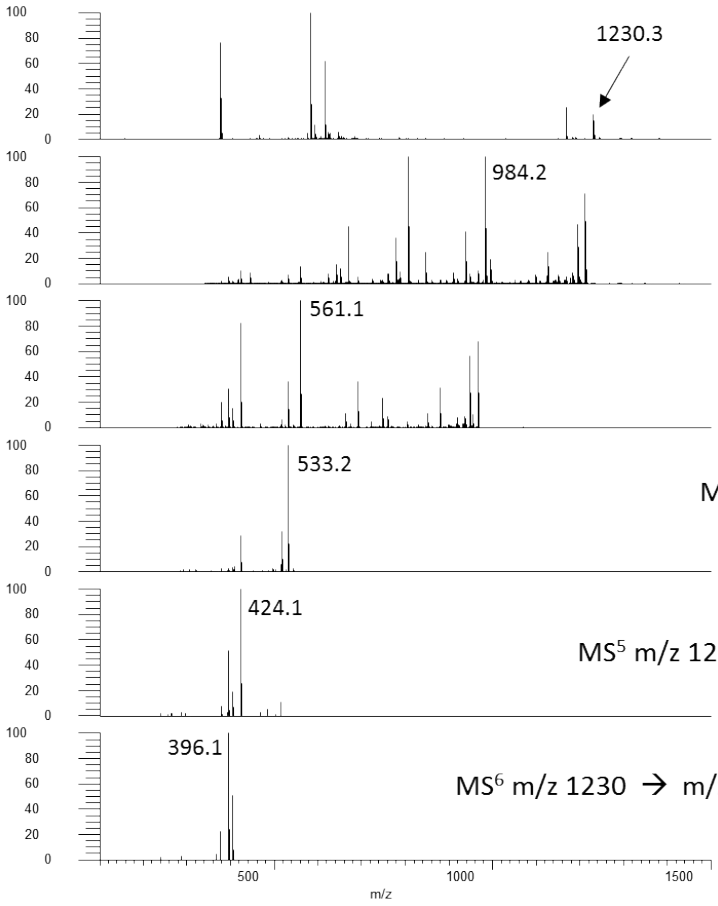


Full ESI(+) spectrum of **[Cu$^{I}$(h-Ctr1_10)]$^{+}$**

MS$^{2}$ m/z 1230 **[Cu$^{I}$(h-Ctr1_10)]$^{+}$**

MS$^{3}$ m/z 1230 → m/984

MS$^{4}$ m/z 1230 → m/z 984 → m/z 561

MS$^{5}$ m/z 1230 → m/z 984 → m/z 561 → m/z 533

MS$^{6}$ m/z 1230 → m/z 984 → m/z 561 → m/z 533 → m/z 424

Figure S7b.

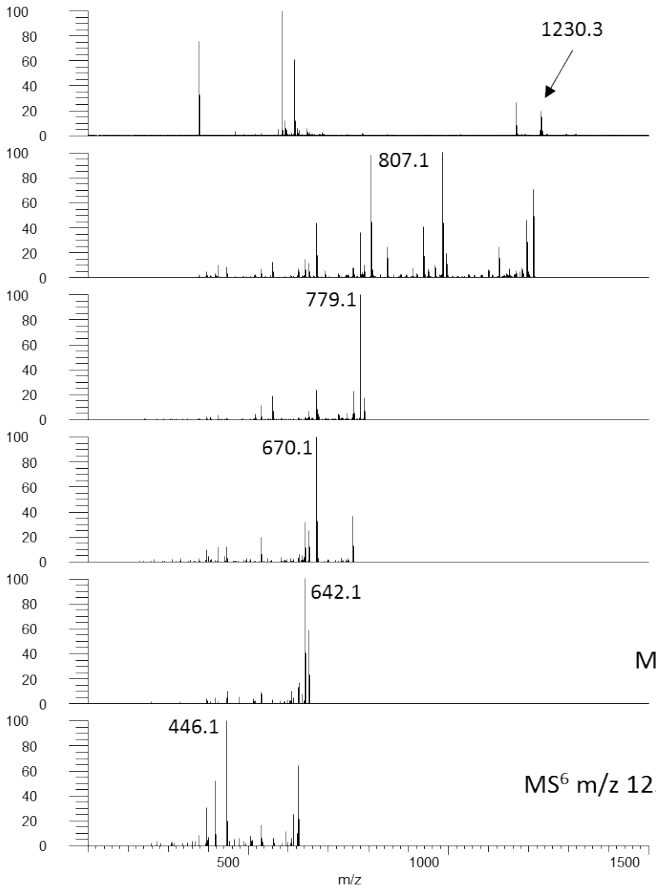


Full ESI(+) spectrum of **[Cu$^{I}$(h-Ctr1_10)]$^{+}$**

MS$^{2}$ m/z 1230 **[Cu$^{I}$(h-Ctr1_10)]$^{+}$**

MS$^{3}$ m/z 1230 → m/z 807

MS$^{4}$ m/z 1230 → m/z 807 → m/z 779

MS$^{5}$ m/z 1230 → m/z 807 → m/z 779 → m/z 670

MS$^{6}$ m/z 1230 → m/z 807 → m/z 779 → m/z 670 → m/z 642

Figure S8.

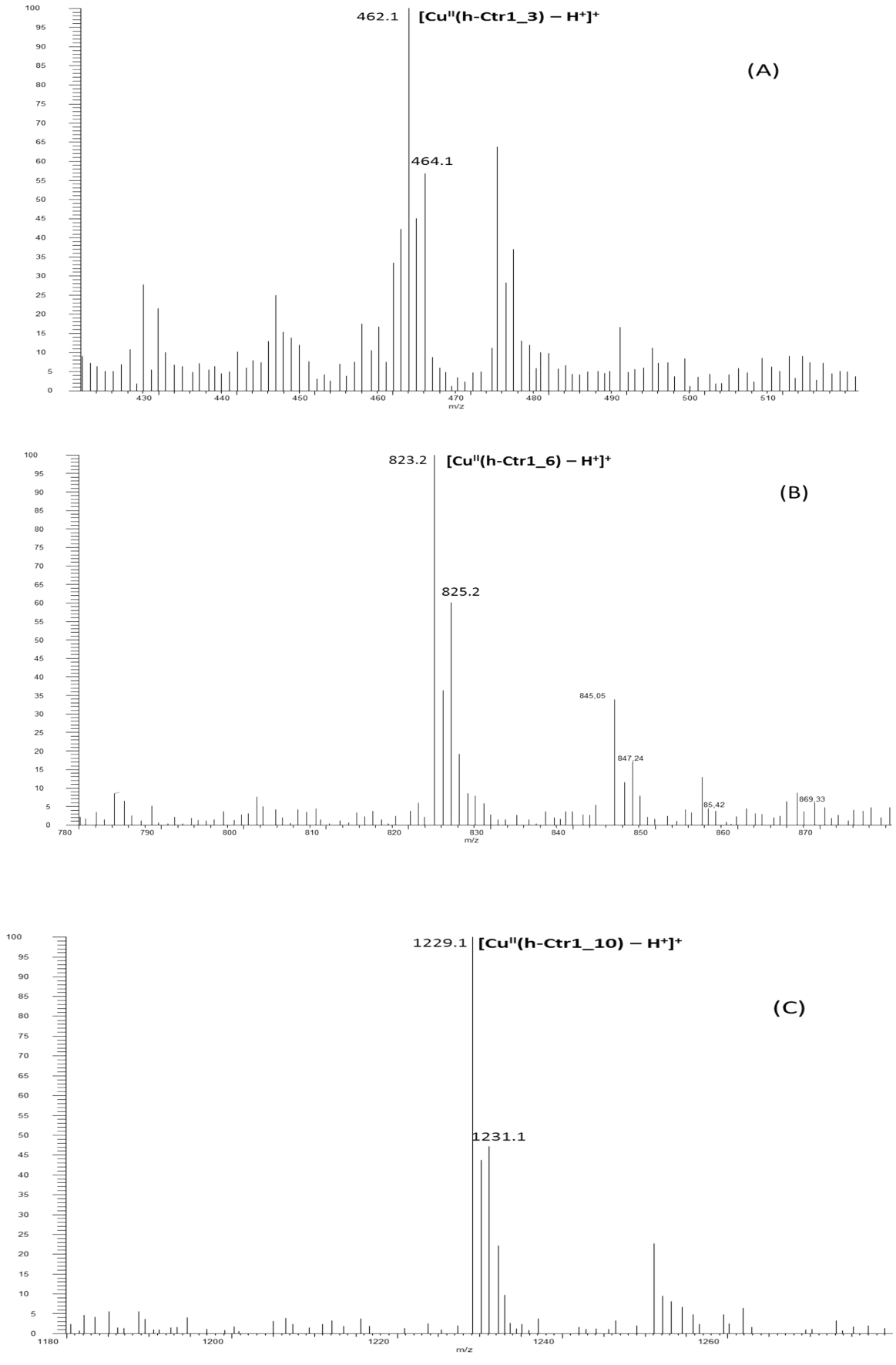
462.1
[Cu$^{II}$(h-Ctr1_3) − H$^+$]$^+$
(A)
464.1
m/z
823.2
[Cu$^{II}$(h-Ctr1_6) − H$^+$]$^+$
(B)
825.2
845,05
847,24
85,42
869,33
m/z
1229.1
[Cu$^{II}$(h-Ctr1_10) − H$^+$]$^+$
(C)
1231.1
m/z

Figure S9.

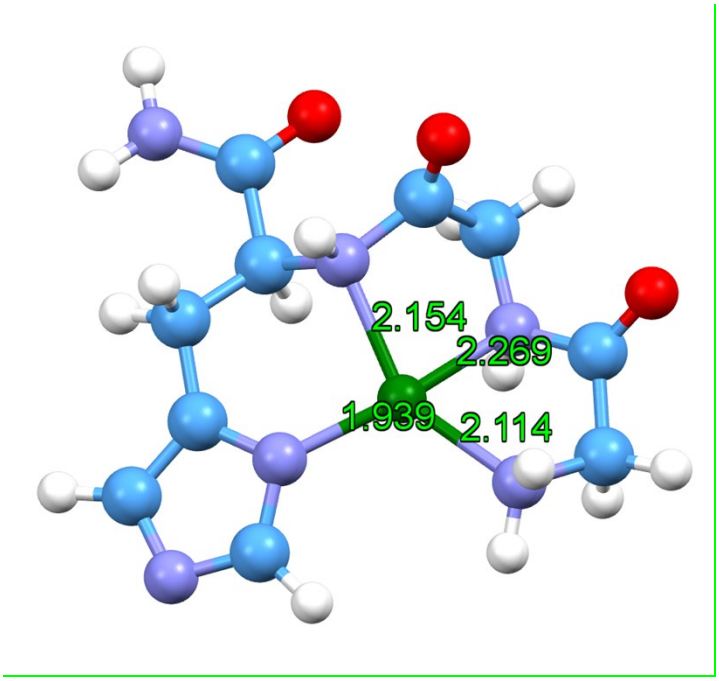

Figure S10.

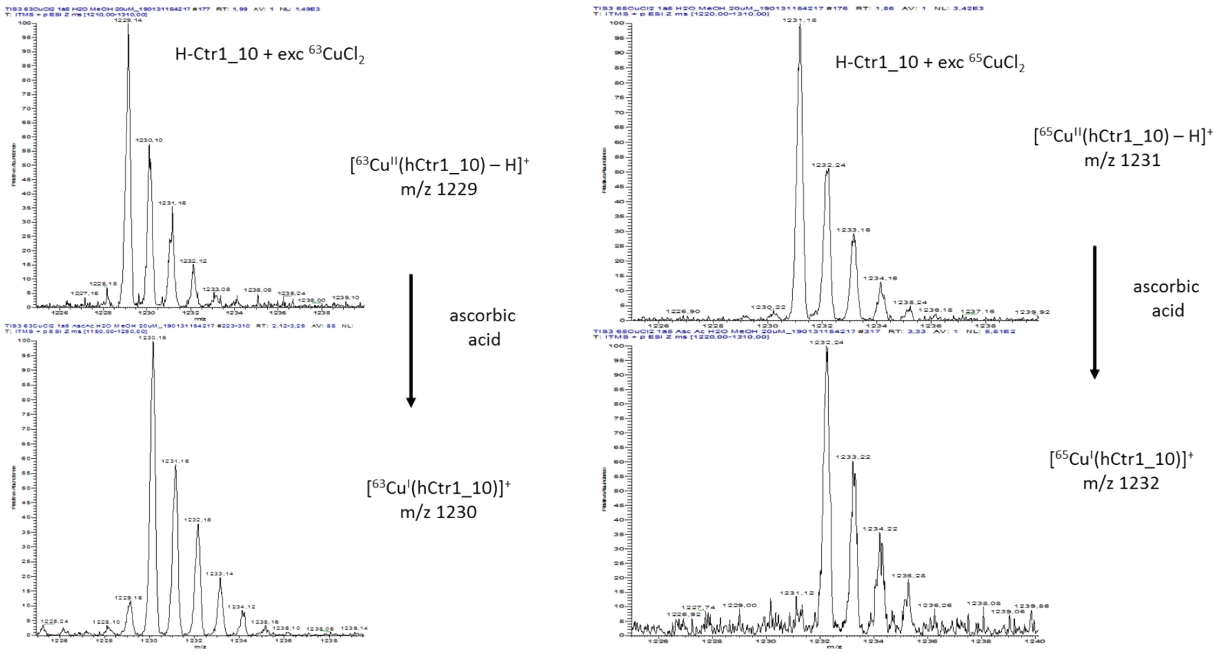
H-Ctr1_10 + exc $^{63}CuCl_2$
$[^{63}Cu^{II}(hCtr1\_10) - H]^+$
m/z 1229
ascorbic acid
$[^{63}Cu^{I}(hCtr1\_10)]^+$
m/z 1230
H-Ctr1_10 + exc $^{65}CuCl_2$
$[^{65}Cu^{II}(hCtr1\_10) - H]^+$
m/z 1231
ascorbic acid
$[^{65}Cu^{I}(hCtr1\_10)]^+$
m/z 1232

Figure S11.

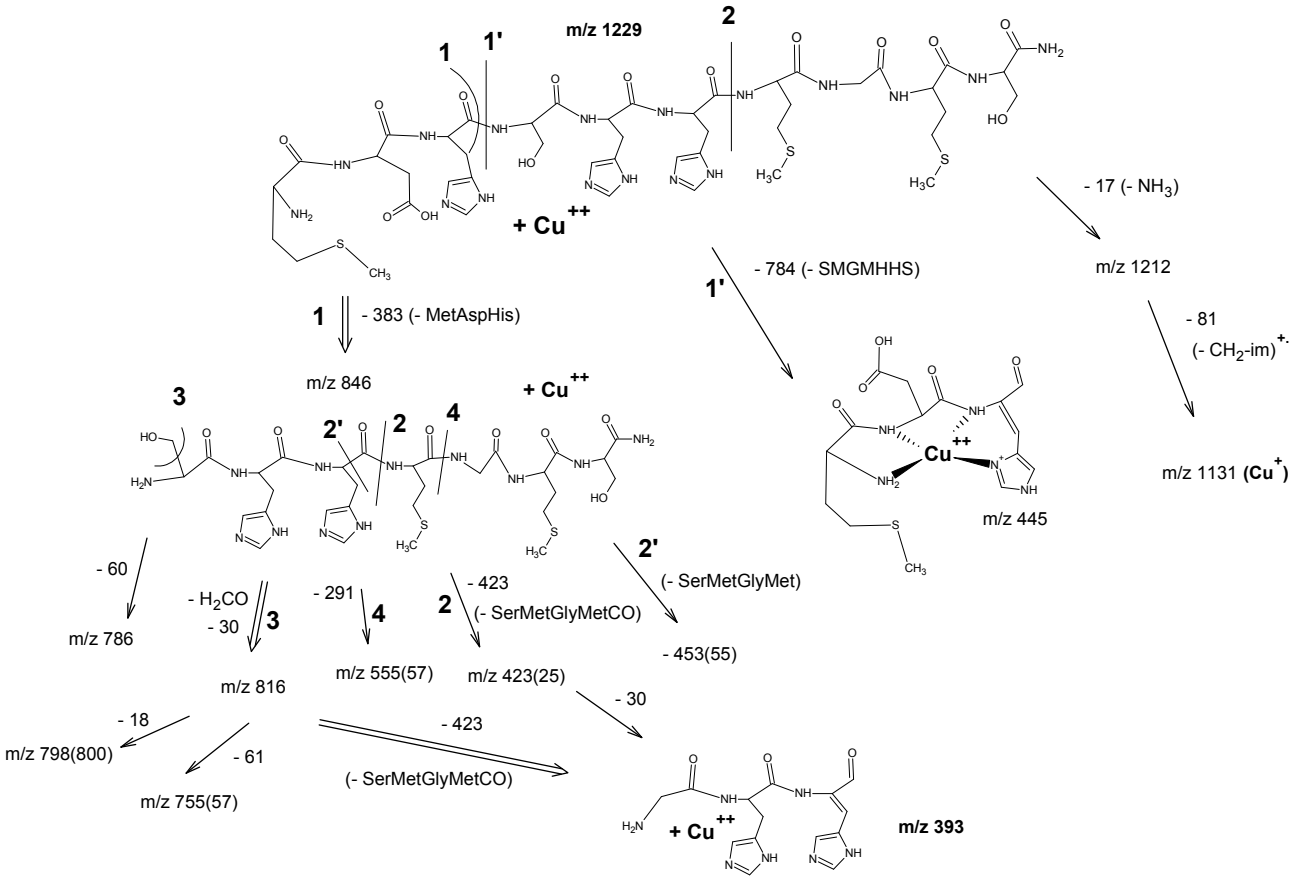
m/z 1229
1
1'
2
+ Cu++
- 17 (- NH3)
m/z 1212
- 81
(- CH2-im)+.
m/z 1131 (Cu+)
- 784 (- SMGMHHS)
m/z 445
Cu++
- 383 (- MetAspHis)
m/z 846
3
2'
2
4
+ Cu++
- 60
m/z 786
- H2CO
- 30
3
m/z 816
- 291
4
m/z 555(57)
2
- 423
(- SerMetGlyMetCO)
m/z 423(25)
2'
(- SerMetGlyMet)
- 453(55)
- 30
- 18
m/z 798(800)
- 61
m/z 755(57)
- 423
(- SerMetGlyMetCO)
+ Cu++
m/z 393

Figure S12.

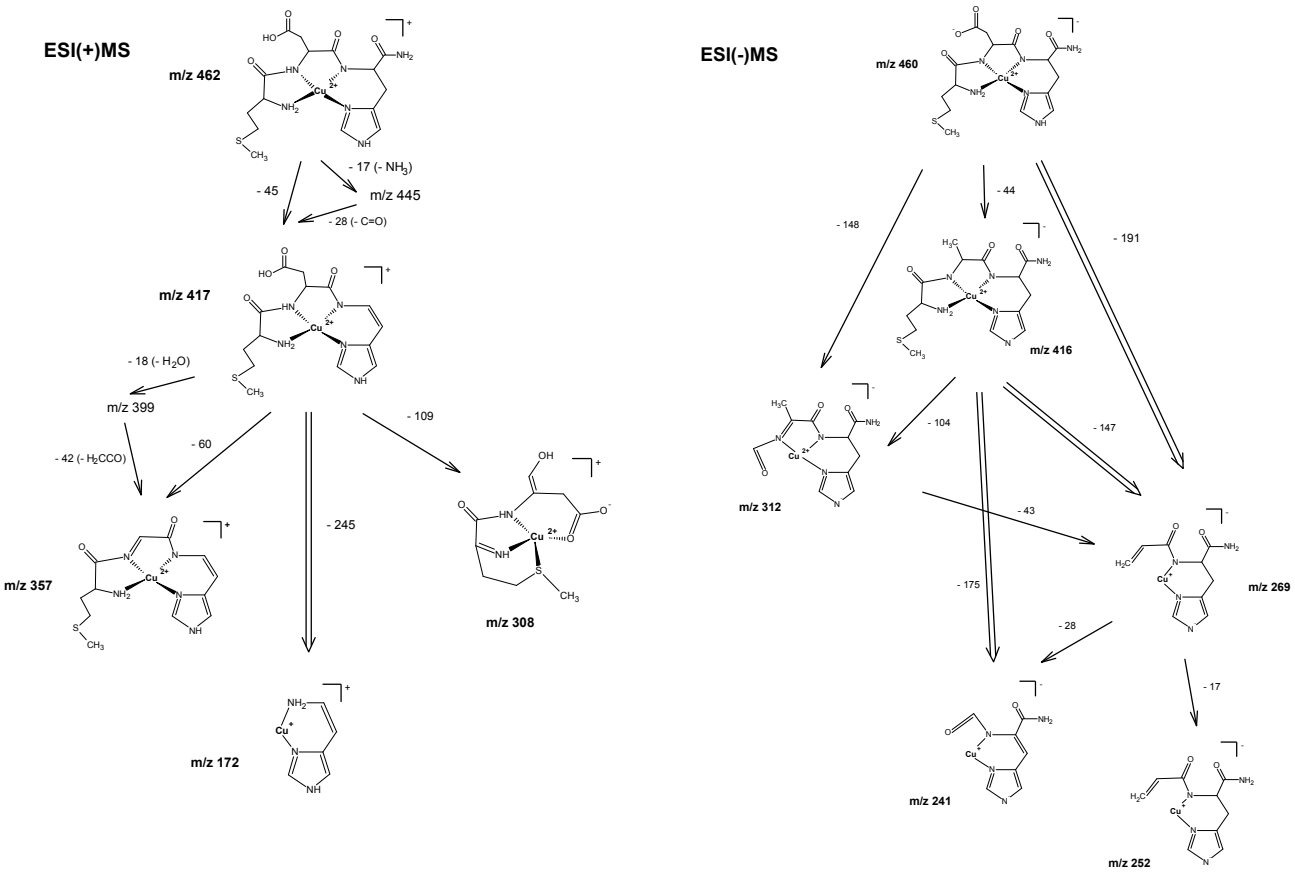
ESI(+)MS
m/z 462
- 17 (- NH3)
- 45
m/z 445
- 28 (- C=O)
m/z 417
- 18 (- H2O)
m/z 399
- 42 (- H2CCO)
- 60
- 109
- 245
m/z 357
m/z 308
m/z 172
ESI(-)MS
m/z 460
- 44
- 148
- 191
m/z 416
- 104
- 147
m/z 312
- 43
- 175
- 28
m/z 269
- 17
m/z 241
m/z 252